Highly efficient Cherenkov radiation in photonic crystal fibers for broadband visible wavelength generation

3 authors, including:

Li-Jin Chen
Massachusetts Institute of Technology
84 PUBLICATIONS **795** CITATIONS

SEE PROFILE

Franz Kärtner
Center for Free-Electron Laser Science
904 PUBLICATIONS **13,734** CITATIONS

SEE PROFILE

Highly efficient Cherenkov radiation in photonic crystal fibers for broadband visible wavelength generation

Guoqing Chang,* Li-Jin Chen, and Franz X. Kärtner

Department of Electrical Engineering and Computer Science and Research Laboratory of Electronics,
Massachusetts Institute of Technology, 77 Massachusetts Avenue, Cambridge, Massachusetts 02139, USA
*Corresponding author: guoqing@mit.edu

We investigate the dependence of Cherenkov radiation (CR) on pump pulse parameters and its evolution along the propagation distance. Using a Ti:sapphire laser emitting 10 fs pulses as the pump source, we demonstrate highly efficient (>40%), broadband (>50 nm) CR in the visible-wavelength range with a threshold energy less than 100 pJ and a tuning range over 100 nm. © 2010 Optical Society of America
OCIS codes: 060.7140, 190.4370, 190.5530.

Fiber-hosted Cherenkov radiation (CR), also known as dispersive wave generation or nonsolitonic radiation, originates from a soliton perturbed by higher order dispersion [1,2]. This intriguing phenomenon has emerged as a wavelength conversion technique to generate significant radiation in the visible-wavelength range, where mode-locked femtosecond lasers are not available [3–7]. The resulting laser source is of importance for applications such as biophotonics, carrier-envelope phase control of ultrashort pulses, and calibration of astrophysical spectrographs using high-precision frequency combs (known as astro-combs [8]). To date, most experimental results have left the impression that CR in the visible-wavelength range forms narrowband spectra ($\sim$10 nm) with relatively low conversion efficiency ($\sim$10%) if pumped with a near-infrared (NIR) laser. While [3] has achieved the highest conversion efficiency of 24%, CR still covers only an $\sim$10 nm bandwidth. In this Letter, we explore the dependence of these two quantities (i.e., conversion efficiency and bandwidth) on the input NIR pulse parameters (such as duration and pulse energy) and demonstrate CR featuring high-efficiency (>40%), broadband emission (>50 nm), and a low threshold (<100 pJ for pulse energy).

Nonlinear evolution of ultrashort pulses inside an optical fiber may be accurately modeled by the generalized nonlinear Schrödinger equation (NLSE) that takes into account dispersion, self-phase modulation, self-steepening, and stimulated Raman scattering [9]. To be consistent with experimental results, we simulated an optical pulse centered at 0.8 μm propagating inside a photonic crystal fiber [(PCF) NL-1.8-710, Crystal Fibre A/S]. As the group-velocity dispersion curve in Fig. 1(a) shows, the fiber exhibits zero dispersion at 0.71 μm. Also plotted in the same figure is the optical spectrum after 2 cm propagation of a hyperbolic-secant pulse with 10 fs FWHM and 300 pJ energy. Clearly, CR has developed an isolated spectrum centered at 0.5 μm determined by the phase-matching condition. Spanning more than 60 nm, this isolated spectrum carries about 40% of the total input power. Figure 1(b) illustrates CR efficiency as a function of input pulse energy for three different pulse FWHM durations. We consider the power distributed between 0.4 μm and 0.6 μm being carried on by CR because the isolated CR spectrum appears in this region for all the simulated cases. The CR efficiency is simply defined as the portion of total

input power converted into the CR spectrum. Three curves in Fig. 1(b) corresponding to 10 fs, 50 fs, and 100 fs follow the same trend: the CR efficiency grows drastically with the increment of input pulse energy and tends to saturate at higher energy levels. These simulations immediately suggest that CR can be a highly efficient (>40%) process if 10 fs level pulses are employed. The broader bandwidth (>60 nm) indicated by Fig. 1(a) constitutes another benefit brought from switching to shorter excitation pulses. These two merits (i.e., high efficiency and broad band) are of particular importance for applications that require larger bandwidth out of relatively weak ultrafast sources.

Guided by the simulation, we have performed a series of experiments on CR from NL-1.8-710 PCF pumped by a homebuilt Ti:sapphire laser operating at 85 MHz
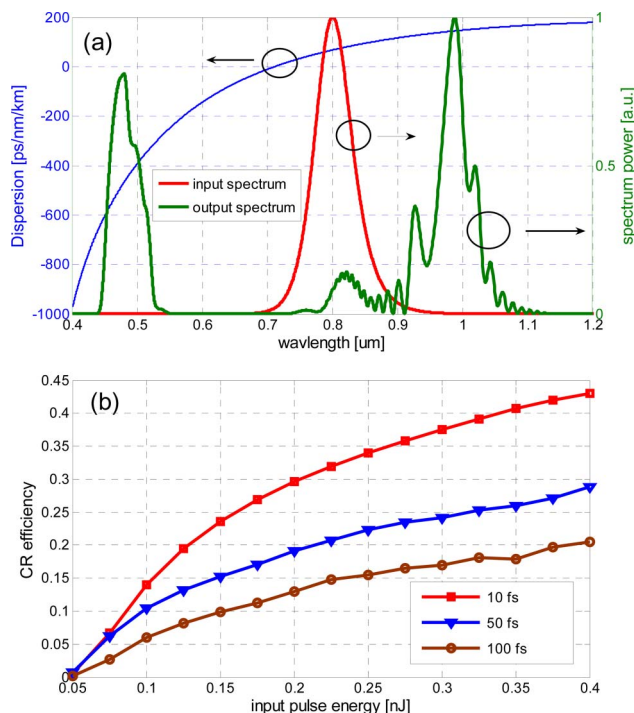

Fig. 1. (Color online) (a) PCF dispersion and pulse spectrum after propagating a 300 pJ, 10 fs pulse through 2 cm PCF and (b) CR efficiency versus input pulse energy for three FWHM durations of the input pulse: 10 fs, 50 fs, and 100 fs.

© 2010 Optical Society of America

repetition rate with ∼10 fs pulse duration. Because the fiber exhibits slight birefringence, we use an achromatic half-wave plate to align the input pulse polarization and ensure a linearly polarized output. The input power is adjusted with a neutral-density filter wheel inserted into the beam path. The dispersion of the neutral-density filter, the achromatic half-wave plate, and the coupling lens to the fiber is compensated by 10 bounces on double-chirped mirrors [10]. Each bounce provides –60 fs^2 group-delay dispersion. The PCF output is collimated and sent into an optical spectrum analyzer (OSA) or a powermeter. To reveal the evolution of CR along the propagation distance inside the fiber, which has not been experimentally studied before, we coupled 300 pJ pulses into PCFs of different lengths and recorded the corresponding spectra in Fig. 2(a). The results suggest three evolution stages corresponding to three fiber length scales: (i) CR within several millimeters, (ii) CR spectral broadening due to self-phase modulation within a few centimeters, and (iii) blueshift and splitting of CR's spectrum due to the decelerating Raman soliton, which normally occurs beyond several centimeters propagation distance.

The location of CR in the first stage is governed by the phase-matching condition [11]:

$$\sum_{n\geq2}\frac{(\omega_{CR}-\omega_p)^n}{n!}\beta_n(\omega_p)=\frac{\gamma P_p}{2},$$

where ω_{CR} and ω_p are the central frequencies of CR and the input NIR pulse. β_n represents the nth order derivative of the propagation constant taken at the frequency ω_p. γ and P_p denote the fiber nonlinear parameter and the pulse peak power, respectively. The diamond-marked blue curve in Fig. 2(b) illustrates the calculated CR location as a function of the input pulse wavelength, assuming a 300 pJ input pulse of 10 fs length. As the input pulse centers at 800 nm, the curve predicts the CR to be located at 500 nm, in agreement with our experimental observation [the curve labeled with 4 mm in Fig. 2(a)]. For comparison, the case neglecting nonlinear phase contribution (i.e., $P_p = 0$) is also plotted as the circle-marked green curve.

It is worth noting that the CR spectrum at the first several millimeters of the PCF manifests as a pulse about 15 fs long in the time domain. Self-phase modulation experienced by such a short pulse during the second stage significantly broadens the CR spectrum and reshapes it into a rectangular shape [the curve labeled 2 cm in Fig. 2(a)]— a characteristic feature attributed to the interaction between self-phase modulation and normal dispersion. The large normal dispersion quickly stretches the pulse to ∼1 ps long within several centimeters of propagation distance; self-phase modulation that is proportional to the pulse peak power becomes minimal. The spectrum bandwidth stays nearly constant until entering the next stage.

Also in the second stage, a Raman soliton forms at the long wavelength and redshifts, driven by stimulated Raman scattering. The interaction between the CR pulse and the Raman soliton relies on their group velocities [7,12]. The inset of Fig. 2(b) plots the wavelength-dependent group velocity defined by the fiber dispersion. Such a quasi-parabolic curve permits two wavelengths
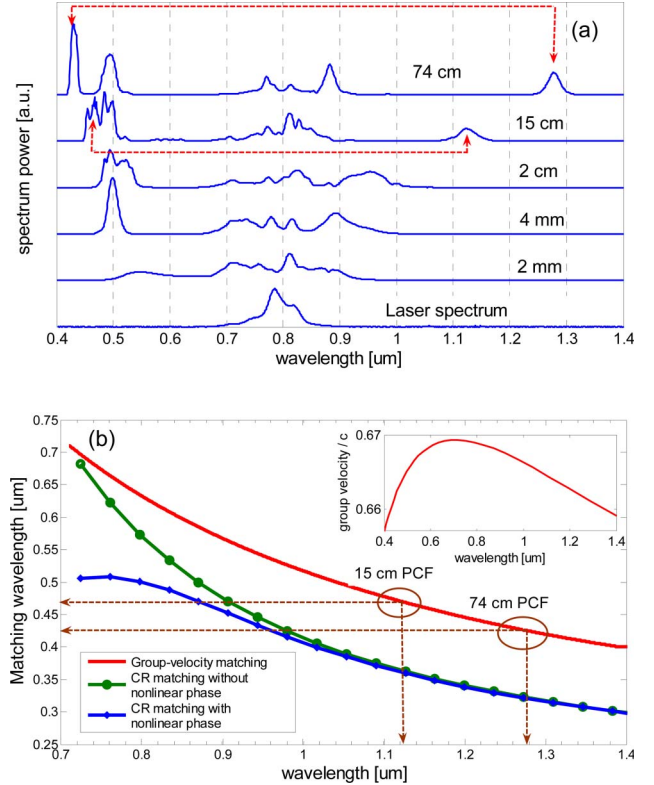

Fig. 2.   (Color online) (a) Evolution of CR with increased PCF length. The input pulse energy is fixed at 300 pJ. Two arrow pairs denote the group-velocity matching wavelengths predicted by the fiber dispersion. (b) Phase-matching condition for CR and group-velocity matching. The matching points between the CR pulse and Raman soliton corresponding to 15 cm and 74 cm PCF are marked, respectively, to illustrate the trapping process. Inset shows the wavelength-dependent group-velocity normalized to the light speed in vacuum.

matching the same group velocity. The nonmarked, red curve in Fig. 2(b) illustrates this group-velocity governed wavelength matching. Apparently, before redshifting to 1.05 μm, the Raman soliton travels faster than the CR pulse centered at 500 nm; no interaction exists due to the large temporal separation. With further propagation, the Raman soliton continues shifting toward the longer wavelength and, therefore, slows down. As the CR pulse eventually catches up with the decelerating Raman soliton, the evolution enters the third stage, in which the Raman soliton traps part of the CR spectrum [the curve labeled with 15 cm in Fig. 2(a)]. Because of the continuous redshifting of the Raman soliton, the group-velocity matching forces the captured CR spectrum to shift toward the shorter wavelength accordingly. As a result, the CR spectrum splits into two well-separated parts [the curve labeled 74 cm in Fig. 2(a)]. The two circles on the group-velocity matching curve in Fig. 2(b) denote the matched wavelengths for the Raman solitons generated in PCFs of 15 cm and 74 cm, respectively. These group-velocity matched wavelengths are identified by the arrow pairs in Fig. 2(a). The theoretical prediction and the experimental observation agree extremely well on the wavelength position of the trapped CR spectrum.

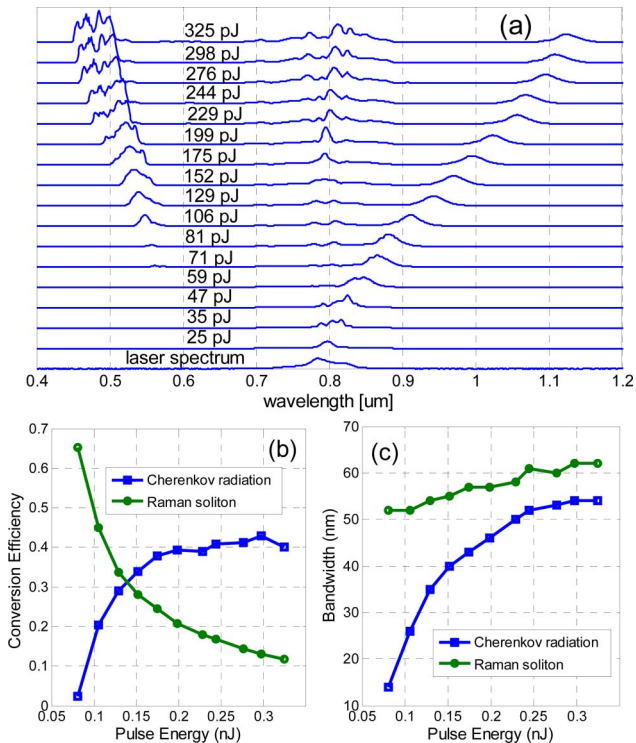The phase-matching condition implies that the CR wavelength depends on the input pulse peak power (or

Fig. 3. (Color online) (a) Evolution of CR and Raman soliton with increased pulse energy for 15 cm PCF, (b) conversion efficiency of CR and Raman soliton versus input pulse energy, and (c) 7 dB bandwidth of CR and Raman soliton versus input pulse energy.

input pulse energy when the pulse duration is fixed). Comparing the circle-marked green curve (phase-matching with nonlinear-phase contribution) with the diamond-marked blue curve (phase-matching neglecting nonlinear phase) in Fig. 2(b) indicates that the CR locates at a shorter wavelength as we increase the input pulse energy. To verify this prediction, we adjusted input pulse energies coupled into a 15 cm PCF and recorded the spectra as shown in Fig. 3(a). As expected, the CR blueshifts with the increment of the input pulse energy. Figures 3(b) and 3(c) summarize the conversion efficiency and 7 dB bandwidth of the CR pulse and Raman soliton. These data clearly revealed three distinct evolution regimes with respect to pulse energies: (i) below 70 pJ, no distinguishable CR is observed, while a Raman soliton has developed; (ii) at 70–200 pJ, CR conversion efficiency and bandwidth grow dramatically with the spectrum approaching rectangular shape due to self-phase modulation and normal dispersion; and (iii) beyond 200 pJ, these two quantities (i.e., conversion efficiency and bandwidth) saturate and stay nearly constant. In this regime, a noticeable dip has developed in the middle of the CR spectrum and becomes deeper with increased input pulse energy—a signature indicating Raman soliton trapping. While its central wavelength undergoes steady redshift as the input pulse becomes stronger, the Raman soliton energy varies marginally, and, therefore, its conversion efficiency drops continuously, as shown in Fig. 3(b). Additionally, the spectra in Fig. 3(a) imply that the aforementioned "three fiber length scales" depend on input pulse energy.

Most important, the data of the above experiments have demonstrated that CR, when pumped with 10 fs pulses of more than 200 pJ pulse energy, exhibits high conversion efficiency (>40%), broad bandwidth (>50 nm), and low threshold (<100 pJ for pulse energy). These three merits allow achieving broadband visible-wavelength spectra from relatively low-energy ultrafast sources, which opens up new applications. For example, scaling up the repetition rate of a Ti:sapphire femtosecond oscillator beyond gigahertz is inevitably accompanied by low pulse energy (<1 nJ). A frequency comb based on such a gigahertz Ti:sapphire laser constitutes a crucial part (known as a "source comb") of an astro-comb that has recently emerged as a enabling tool for precision radial velocity observations [8]. The demonstrated low-threshold CR can efficiently convert such a NIR source comb into its broadband counterpart at the visible-wavelength range. With a proper Fabry–Perot filtering cavity to increase the line spacing of the CR source comb, the resulting astro-comb of visible wavelength holds the promise to locate Earth-like extrasolar planets orbiting around stars similar to the Sun.

In conclusion, we have studied CR along the propagation distance and identified three evolution stages corresponding to three length scales that are dependent on input pulse energy. The highly efficient CR produces broadband (>50 nm) visible-wavelength spectra tunable within over 100 nm (i.e., from 0.45 μm to 0.55 μm) range, controlled by input pulse energy. As is well known, another crucial factor that determines the center wavelength of the CR spectrum is the relative separation between a fiber zero-dispersion wavelength (ZDW) and the input pulse center wavelength. It is anticipated that by switching to PCFs with different ZDW, CR-enabled broadband sources can access the entire visible-wavelength range.

References

1. P. K. A. Wai, C. R. Menyuk, Y. C. Lee, and H. H. Chen, Opt. Lett. **11**, 464 (1986).
2. N. Akhmediev and M. Karlsson, Phys. Rev. A **51**, 2602 (1995).
3. L. Tartara, I. Cristiani, and V. Degiorgio, Appl. Phys. B **77**, 307 (2003).
4. G. Genty, M. Lehtonen, and H. Ludvigsen, Opt. Express **12**, 4616 (2004).
5. A. V. Mitrofanov, Y. M. Linik, R. Buczynski, D. Pysz, D. Lorenc, I. Bugar, A. A. Ivanov, M. V. Alfimov, A. B. Fedotov, and A. M. Zheltikov, Opt. Express **14**, 10645 (2006).
6. H. Tu and S. A. Boppart, Opt. Express **17**, 9858 (2009).
7. S. Hill, C. E. Kuklewicz, U. Leonhardt, and F. Konig, Opt. Express **17**, 13588 (2009).
8. C.-H. Li, A. J. Benedick, P. Fendel, A. G. Glenday, F. X. Kärtner, D. F. Phillips, D. Sasselov, A. Szentgyorgyi, and R. L. Walsworth, Nature **452**, 610 (2008).
9. G. P. Agrawal, *Nonlinear Fiber Optics*, 3rd ed. (Academic, 2001).
10. N. Matuschek, F. X. Kärtner, and U. Keller, IEEE J. Sel. Top. Quantum Electron. **5**, 1385 (1999).
11. A. V. Husakou and J. Herrmann, J. Opt. Soc. Am. B **19**, 2171 (2002).
12. A. V. Gorbach and D. V. Skryabin, Nat. Photon. **1**, 653 (2007).